Hydrogen Production by Sorption-Enhanced Steam Glycerol Reforming: Sorption Kinetics and Reactor Simulation

Ion Iliuta, Hamid R. Radfarnia, and Maria C. Iliuta
Dept. of Chemical Engineering, Laval University, Québec G1V 0A6, Canada

DOI 10.1002/aic.13979
Published online December 26, 2012 in Wiley Online Library (wileyonlinelibrary.com).

Sorption-enhanced glycerol reforming, an integrated process involving glycerol catalytic steam reforming and in situ *CO_2 removal, offers a promising alternative for single-stage hydrogen production with high purity, reducing the abundant glycerol by-product streams. This work investigates this process in a fixed-bed reactor, via a two-scale, nonisothermal, unsteady-state model, highlighting the effect of key operating parameters on the process performance. CO_2 adsorption kinetics was investigated experimentally and described by a mathematical reaction-rate model. The integrated process presents an opportunity to improve the economics of green hydrogen production via an enhanced thermal efficiency process, the exothermic CO_2 adsorption providing the heat to endothermic steam glycerol reforming, while reducing the capital cost by removing the processing steps required for subsequently CO_2 separation. The operational time of producing high-purity hydrogen can be enhanced by increasing the adsorbent/catalyst volume ratio, by adding steam to the reaction system and by increasing the inlet reactor temperature.* *AIChE J,* 59: 2105–2118, 2013
Keywords: sorption-enhanced steam glycerol reforming, in situ *CO_2 removal, CO_2 capture kinetics, modeling*

Introduction

Due to the increasing demand of energy and strained tapping of fossil fuel reserves the use of renewables as a source of hydrogen production has become more and more important during the last few years.[1–5] Glycerol is a promising source for hydrogen production. Glycerol is a significant byproduct during the conversion of vegetable oils or animal fats into biodiesel fuel through the catalytic transesterification process, a process that is undergoing a boom through the building of new biorefineries worldwide as part of the global efforts to combat climate change and reduce dependency on fossil fuel imports.[6–8] The glycerol by-product is now in surplus and could even become a waste problem. For example, Canada alone is expected to produce 55 million liters of glycerol annually.[9]

Glycerol to hydrogen conversion processes can be categorized into two major approaches: aqueous-phase reforming and gas-phase (steam) reforming. Aqueous-phase reforming process was established by Cortright et al.[1] using platinum-based catalysts and moderate reaction conditions (200–250°C and 2–2.5 MPa). Aqueous-phase reforming occurs at conditions that favor water–gas shift reaction, making it possible to generate hydrogen with low amounts of CO in a single-stage reactor. Moreover, low temperatures minimize undesirable decomposition reactions that typically occur at high temperatures. Some limitations of this process are high pressure requirement and low H_2 selectivity (due to the possibility of alkane formation at low temperature).[8] Steam reforming process is a vapor-phase catalytic reaction that occurs at atmospheric pressure and high temperature (600–800°C) using catalysts based on nickel, cobalt, or noble metals. The most important parameters in the glycerol steam reforming process are temperature, steam-to-carbon ratio, and catalyst-to-feed ratio. Major concerns are by-product formation (e.g., CO), catalyst deactivation, and high energy consumption. Other processes, including autothermal reforming,[10] thermal decomposition,[11,12] catalytic partial oxidation process,[13] bioconversion using genetically engineered enzymes, photocatalytic, electrochemical, and hydrogen peroxide reforming,[14] have been investigated, too. Among these processes, steam reforming of glycerol has attracted much more attention, as it can produce up to 7 mol of hydrogen per mole feed glycerol theoretically via the overall reaction

$$C_3H_5(OH)_3 + 3H_2O \leftrightarrow 3CO_2 + 7H_2 \qquad \Delta H = 128\text{kJ/mol} \tag{1}$$

This reaction may be viewed as the combination of:

$$C_3H_5(OH)_3 \leftrightarrow 3CO + 4H_2 \text{ (glycerol decomposition)} \tag{1a}$$

$$CO + H_2O \leftrightarrow CO_2 + H_2 \text{ (water-gas shift reaction)} \tag{1b}$$

However, it may also be accompanied by CH_4 production and carbon deposition. Indeed, under steam reforming conditions, other thermodynamically feasible reactions can be included

$$2C_3H_5(OH)_3 + H_2 \leftrightarrow 3CH_4 + 3CO + 3H_2O \tag{1c}$$

$$C_3H_5(OH)_3 + 2H_2 \leftrightarrow 2CH_4 + CO + 2H_2O \tag{1d}$$

Correspondence concerning this article should be addressed to M. C. Iliuta at maria-cornelia.iliuta@gch.ulaval.ca.

$$CO + 3H_2 \leftrightarrow CH_4 + H_2O \quad (1e)$$

$$CO_2 + 4H_2 \leftrightarrow CH_4 + 2H_2O \quad (1f)$$

$$CO_2 + CH_4 \leftrightarrow 2CO + 2H_2 \quad (1g)$$

$$CH_4 \leftrightarrow 2H_2 + C(s) \quad (1h)$$

$$C(s) + H_2O \leftrightarrow CO + H_2 \quad (1i)$$

$$2CO \leftrightarrow CO_2 + C(s) \quad (1j)$$

One of the difficulties associated with the utilization of the syngas produced by glycerol steam reforming process is the high CO_2 and CO content. Especially for all fuel cell systems, large CO_2 content of the fuel gas greatly declines the efficiency of the system, whereas CO has very strong poisoning effect on the catalyst.[15] The conventional CO_2 and CO cleanup from the steam reforming reactor is a very costly and complicated process.[16] In recent years, a new concept involving simultaneous hydrogen production and *in situ* CO_2 removal by adsorption has been proposed. This process is well known as the sorption-enhanced reaction process and has been widely studied for steam methane reforming.[16–29] An analysis of these studies shows that sorption-enhanced steam reforming process for H_2 production has the following potential advantages over the conventional reforming process: (1) high-purity hydrogen production in a single step, (2) simplification of the hydrogen production process, (3) no supplemental energy for the primary reactor and reduction of the heat exchangers, (4) reduction of primary reactor operating temperature, which may reduce energy usage and catalyst sintering, (5) less expensive reactor materials,[16,18,22,25] and (6) the reduction of the capital cost of the processing steps required for subsequently CO_2 separation are removed.[16,17,20]

To date, little has been found in the literature on glycerol steam reforming with *in situ* CO_2 removal process. Dou et al.[7,11] found that sorption-enhanced steam glycerol reforming process is an effective means for achieving hydrogen purity above 95% (dry basis). Chen et al.[30] studied the effect of temperature, pressure, steam-to-glycerol molar ratio, CO_2 adsorption fraction, and N_2 dilution on glycerol steam reforming coupled with CO_2 adsorption via thermodynamic calculation. Li et al.[31] investigated the thermodynamic equilibrium of glycerol steam reforming with carbon dioxide sequestration using Gibbs energy minimization method. The influence of the reaction temperature and pressure, $H_2O/C_3H_8O_3$ molar ratio, and $CaO/C_3H_8O_3$ molar ratio on the reaction system was analyzed. Coke formation and energy efficiency of reactions were also discussed. However, with regard to hydrogen production from glycerol steam reforming with *in situ* CO_2 removal process, there are still many challenges regarding the optimization of the process, that is, the selection of the catalyst for the sorption-enhanced steam reforming reactions, the operating temperature, and steam-to-glycerol ratio.

This work investigates the hydrogen production from glycerol into a fixed-bed reactor via an integrated process involving steam glycerol reforming and *in situ* CO_2 removal, highlighting the effect of the key operating parameters on the process performance. A two-scale, nonisothermal, unsteady-state model has been developed to account for gas dynamics whereupon were tied steam glycerol reforming/CO_2 capture kinetics, thermodynamics, thermal effects, and variable gas flow rate due to chemical and physical contractions. The kinetics of CO_2 capture has been investigated experimentally on a CaO material recently developed in our laboratory from natural limestone and described by a mathematical reaction-rate model. CaO-based adsorbent was chosen due to the very fast CO_2 sorption kinetics and low price.[16,28] Moreover, the novel Ca-based adsorbent showed favorable stability and CO_2 sorption capacity upon multicycle operation, which motivated us to study its application in reforming process integrated with *in situ* CO_2 capture.

The integrated process is intended to minimize the abundant glycerol by-product streams via an energy efficient alternative for producing hydrogen. It presents an opportunity to improve the economics of green hydrogen production via an enhanced thermal efficiency process, exothermic CO_2 adsorption providing the heat to endothermic steam glycerol reforming, while reducing the capital cost as the processing steps required for subsequently CO_2 separation are removed.

Experimental

To obtain high-purity CaO material, natural limestone (1.035 g, Newfoundland, Canada), containing CaO 52.9%, MgO 0.27%, Na_2O 1.55%, SiO_2 0.27%, Al_2O_3 0.08%, Fe_2O_3 0.13%, K_2O 0.04%, and loss of ignition 44.8% [obtained from X-ray fluorescence (XRF) analysis], was initially treated by citric acid (1.42 g, 99.5%, Lab Mat) followed by adjusting pH of solution to about 7 using aqueous ammonia to minimize precipitate solubility. The precipitate was centrifuged and dried overnight at 70–75°C, followed by calcination in air at 850°C for 2 h at heating/cooling rates of 10°C/min to obtain fine CaO powder. A detailed CO_2 capture study of citric acid treated limestone was provided elsewhere (Radfarnia et al., submitted for publication). Briefly, about 30 mg of sample was loaded into a Intelligent Gravimetric Analyzer, IGA-003 (Hiden Isochema) and initially heated at 750°C (ramp rate of 8°C/min) for 10 min in pure argon (99.999%, Praxair; 150 mL/min) to perform complete regeneration. The temperature was then set at the desirable carbonation temperature (ramp rate of 8°C/min), and once the temperature was stabilized, the flow was switched to different CO_2 (99.999%, Praxair) partial pressures between 0.15 and 1 bar. CO_2 was balanced with argon stream (total flow rate of 150 mL/min). The carbonation temperatures on cyclic operation (18 cycles) were set between 550 and 700°C. After 30 min adsorption, the samples were regenerated by calcination (decarbonation) at 750°C for 30 min under pure argon. Similar regeneration conditions are extensively applied in the literature for CaO-based adsorbents.[32–34] Synthesized samples were characterized by X-ray diffraction (Siemens powder X-ray diffractometer D5000) and scanning electron microscopy (JEOL JSM-840A).

Development of kinetic model for CO_2 capture

Molar conversion of CaO-based sorbent for the 18th sorption cycle is presented in Figure 1 at different CO_2 partial pressures and carbonation temperatures. It can be seen that the carbonation process comprises a fast step, controlled by the chemisorption process, and a slow step, controlled by CO_2 diffusion. The conversion is almost independent of CO_2 partial pressure, but strongly affected by the carbonation temperature. The increase in carbonation temperature results in the extension of the fast reaction step, thus, increasing the material absorption capacity due to the increase of chemisorption kinetics at elevated temperatures.

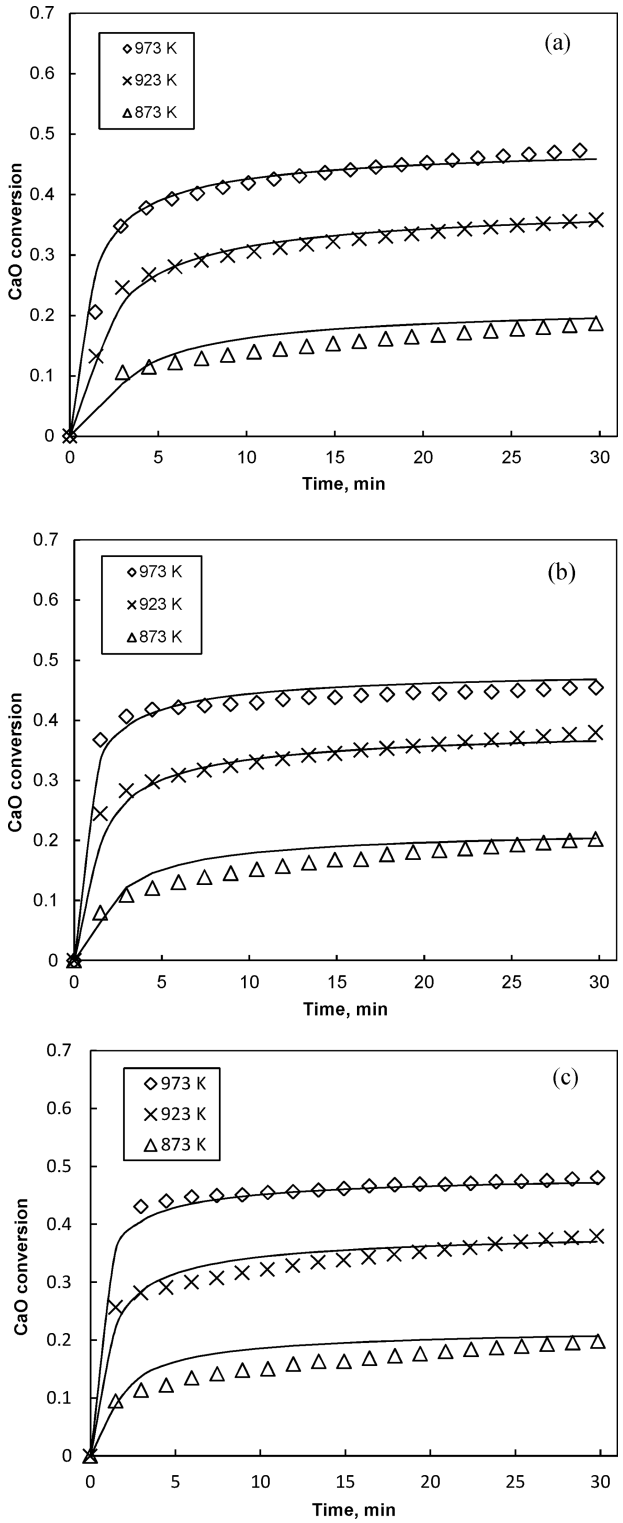

Figure 1. Conversion of Ca-based sorbent for the cycle 18 under 0.15–1 bar at different sorption temperatures—experimental data and kinetic model (lines): (a) 0.15 bar; (b) 0.5 bar; and (c) 1 bar.

Based on the experimental sorption data, a typical model for noncatalytic gas–solid reactions was proposed to describe the kinetics of CO_2 capture on the Ca-based adsorbent[35]

$$\frac{dX}{dt} = k_c f_1(X) f_2(C_{CO_2}) \tag{2}$$

Different gas–solid reaction models (the commonly applied being shrinking unreacted core model, random pore model, and volumetric particle model) were used to evaluate the expression $f_1(X)$. However, shrinking-core model and several other models failed to explain the results obtained in our experiments.

The following expression[35,36] $f_1(X) = (1 - X/X_u)^n$, with $n = 2.61$, which does not explain the capture mechanism, but indicates that the rate-limiting step is changing with fractional conversion gave the best fit of the experimental data. Also, a nonlinear dependency on the CO_2 concentration was found and modeled using the following expression[37] $f_2(C_{CO_2}) = \left(C_{CO_2} - C_{CO_2,eq}\right)^m$, with $m = 0.37$. Similar to the function of fractional conversion, this expression indicates that the rate-limiting step change with CO_2 partial pressure.

Finally, the kinetic model that describes CO_2 capture is

$$\frac{dX}{dt} = k_c\left(C_{CO_2} - C_{CO_2,eq}\right)^{0.37}(1 - X/X_u)^{2.61} \tag{3}$$

For repeated capture-regeneration, the kinetic model becomes

$$\frac{dX_N}{dt} = k_c\left(C_{CO_2} - C_{CO_2,eq}\right)^{0.37}\left(1 - \frac{X_N}{X_{u,N}}\right)^{2.61} \tag{4}$$

where X_N and $X_{u,N}$ denote the fractional conversion and ultimate conversion of Ca-based adsorbent in Nth sorption cycle, respectively.

The semiempirical equation developed by Grasa and Abanades[38] was used to describe the Ca-based adsorbent conversion loss with the number of cycles

$$X_{u,N} = \frac{1}{\frac{1}{1-X_r} + k_r N} + X_r \tag{5}$$

X_r is the residual conversion of Ca-based adsorbent after many cycles, and k_r is the deactivation constant

$$X_r = -0.167811\left(\frac{T}{100}\right)^2 + 0.033211 \times T - 15.992 \tag{6}$$

$$k_r = 3.5 \times 10^5 \exp(-0.01327 \times T) \tag{7}$$

For the kinetic constant k_c, an Arrhenius expression was used to describe the temperature dependence

$$k_c = 1.106 \times 10^6 \exp\left(-\frac{17,937.18}{T}\right) \tag{8}$$

The equilibrium partial pressure of CO_2 (bar) as a function of temperature was evaluated as[39]

$$P_{CO_2,eq} = 1.01325 \times 10^{\left(-\frac{8308}{T} + 7.079\right)} \tag{9}$$

Sorption-enhanced steam glycerol reforming fixed-bed reactor model

A two-scale, nonisothermal, unsteady-state model was developed to analyze the application of the concept of CO_2

removal by adsorption during the steam glycerol reforming process. A transient model is chosen, because the capture of CO_2 has a time-dependent nature, and axial dispersion is included, because relatively low gas velocities are used in the simulations. The model considers that CO_2 capture and reforming processes take place in two different particles: the fixed-bed reactor is packed with a mixture of catalytic particles for glycerol reforming and adsorbent particles for CO_2 adsorption (CO_2 is the only adsorbed species; the adsorption of water on Ca-based absorbent was not considered, because the formation of calcium hydroxide is not significantly active in the conditions considered in this work, due to its low stability[7,28]). The catalyst and adsorbent form a homogeneous mixture of monodisperse particles. The contribution of the reaction and adsorption was weighted according to the volume fraction of the corresponding functionalities.

Bulk Scale Model—Mass, Momentum, and Heat Transport Equations. Unsteady-state mass, momentum, and enthalpy balance equations in the bulk gas phase are written as follows:

Species mass balance equations

$$\varepsilon_g \frac{\partial}{\partial t}\left(P_{j,g}\right) + \varepsilon_g \frac{\partial}{\partial z}\left(u_g P_{j,g}\right) = D_{g,j}\varepsilon_g \frac{\partial^2 P_{j,g}}{\partial z^2} - D_{j,cat}^{eff} \frac{\partial P_{j,cat}}{\partial r}\bigg|_{r=r_p} a_{s,cat} f_{cat}(1-\varepsilon) \quad (10)$$

where $j = H_2$, $C_3H_8O_3$, and H_2O

$$\varepsilon_g \frac{\partial}{\partial t}\left(P_{CO_2,g}\right) + \varepsilon_g \frac{\partial}{\partial z}\left(u_g P_{CO_2,g}\right) = D_{g,CO_2}\varepsilon_g \frac{\partial^2 P_{CO_2,g}}{\partial z^2} - D_{CO_2,cat}^{eff} \frac{\partial P_{CO_2,cat}}{\partial r}\bigg|_{r=r_p} a_{s,cat} f_{cat}(1-\varepsilon) - D_{CO_2,ads}^{eff} \frac{\partial P_{CO_2,ads}}{\partial r}\bigg|_{r=r_p} a_{s,ads} f_{ads}(1-\varepsilon) \quad (11)$$

Overall mass balance equation

$$\frac{\partial}{\partial t}\left(\varepsilon_g \rho_g\right) + \frac{\partial}{\partial z}\left(u_g \varepsilon_g \rho_g\right) = \rho_{sc} M_g \sum_i \sum_j v_{ij}\eta_i r_i \quad (12)$$

Momentum balance equation

$$\frac{\partial}{\partial t}\left(\rho_g \varepsilon_g u_g\right) + u_g \frac{\partial}{\partial z}\left(\rho_g \varepsilon_g u_g\right) = -\varepsilon_g \frac{\partial P}{\partial z} - \left[180\frac{\left(1-\varepsilon_g\right)^2}{\varepsilon_g^3 d_p^2}\mu_g v_{sg} + 1.8\frac{1-\varepsilon_g}{\varepsilon_g^3 d_p}\rho_g v_{sg}^2\right]\varepsilon_g \quad (13)$$

Average heat balance equation

$$\left[\varepsilon_g \rho_g c_{pg} + \rho_{sc} c_{ps}\right]\frac{\partial T}{\partial t} + \varepsilon_g \rho_g u_g c_{pg}\frac{\partial T}{\partial z} = \lambda_z^{eff}\frac{\partial^2 T}{\partial z^2} - \lambda_{cat}^{eff}\frac{\partial T_{cat}}{\partial r}\bigg|_{r=r_p} a_{s,cat} f_{cat}(1-\varepsilon) - \lambda_{ads}^{eff}\frac{\partial T_{ads}}{\partial r}\bigg|_{r=r_p} a_{s,ads} f_{ads}(1-\varepsilon) - \frac{4K_T}{d}(T - T_w) \quad (14)$$

Initial and boundary conditions for mass, momentum, and heat balance equations are as follows

$$t = 0, z > 0 \quad u_g = u_g^{in}, P = P^{in}, P_{j,g} = P_{j,g}^{in}, T = T^{in} \quad (15)$$

where $j = C_3H_8O_3$, H_2O, H_2, and CO_2

$$t > 0, z = 0 \quad u_g = u_g^{in},\ P = P^{in}, \quad u_g P_{j,g}\big|_{z=0^-} = u_g P_{j,g}\big|_{z=0^+} - D_{g,j}\frac{\partial P_{j,g}}{\partial z}\bigg|_{z=0} \quad (16)$$

$$u_g \varepsilon_g \rho_g c_{pg} T\big|_{z=0^-} = u_g \varepsilon_g \rho_g c_{pg} T\big|_{z=0^+} - \varepsilon_g \lambda_z^{eff}\frac{\partial T}{\partial z}\bigg|_{z=0} \quad (17)$$

$$t > 0, z = H \quad \frac{\partial P_{j,g}}{\partial z}\bigg|_{z=H} = 0 \quad \frac{\partial T}{\partial z}\bigg|_{z=H} = 0 \quad (18)$$

P, ε_g, ρ_g, and u_g represent, respectively, pressure, void volume fraction, gas density, and interstitial gas velocity. $P_{j,g}$ is the partial pressure of species j in the gas phase. The second term in the right side of Eq. 13 represents the interfacial drag force per unit reactor volume. $\eta_i\lambda$ is the effectiveness factor of reaction i and is calculated as the ratio between the reaction rate with pore diffusion and heat resistance, obtained from integration of the intrinsic reaction rate along the radial coordinate within the catalyst particle, and the reaction rate at the gas bulk temperature and concentrations

$$\eta_i = \frac{\int_v r_i dV}{r_i\big|_g} \quad (19)$$

The average apparent density of the catalyst and adsorbent in the reactor, ρ_{sc}, can be written as

$$\rho_{sc} = \rho_p^{cat} f_{cat}(1-\varepsilon) + \rho_p^{ads} f_{ads}(1-\varepsilon) \quad (20)$$

Porous Catalyst Particle Scale Model—Mass and Heat Balance Equations. The solution of the bulk scale model equations requires knowledge of the concentration and temperature profiles inside the catalyst particles. These concentration and temperature gradients are given by the equations describing the simultaneous mass and heat transport and reaction within the catalyst particles (convective terms are assumed to be insignificant)

$$\varepsilon_p^{cat}\frac{\partial P_{H_2}^{cat}}{\partial t} = D_{H_2,cat}^{eff}\frac{1}{r^2}\frac{\partial}{\partial r}\left(r^2\frac{\partial P_{H_2}^{cat}}{\partial r}\right) + 7\rho_p^{cat} r_{ref} R T_{cat} \quad (21)$$

$$\varepsilon_p^{cat}\frac{\partial P_{CO_2}^{cat}}{\partial t} = D_{CO_2,cat}^{eff}\frac{1}{r^2}\frac{\partial}{\partial r}\left(r^2\frac{\partial P_{CO_2}^{cat}}{\partial r}\right) + 3\rho_p^{cat} r_{ref} R T_{cat} \quad (22)$$

$$\varepsilon_p^{cat}\frac{\partial P_{H_2O}^{cat}}{\partial t} = D_{H_2O,cat}^{eff}\frac{1}{r^2}\frac{\partial}{\partial r}\left(r^2\frac{\partial P_{H_2O}^{cat}}{\partial r}\right) - 3\rho_p^{cat} r_{ref} R T_{cat} \quad (23)$$

$$\varepsilon_p^{cat}\frac{\partial P_{C_3H_8O_3}^{cat}}{\partial t} = D_{C_3H_8O_3,cat}^{eff}\frac{1}{r^2}\frac{\partial}{\partial r}\left(r^2\frac{\partial P_{C_3H_8O_3}^{cat}}{\partial r}\right) - \rho_p^{cat} r_{ref} R T_{cat} \quad (24)$$

$$\left(\varepsilon_p^{cat}\rho_g c_{pg} + \rho_p^{cat} c_{ps}\right)\frac{\partial T_{cat}}{\partial t} = \lambda_{cat}^{eff}\frac{1}{r^2}\frac{\partial}{\partial r}\left(r^2\frac{\partial T_{cat}}{\partial r}\right) + (-\Delta H_{R,ref}) r_{ref}\rho_p^{cat} \quad (25)$$

The corresponding boundary and initial conditions are given as

$$t > 0, r = r_{\mathrm{p}}^{\mathrm{cat}} \quad D_{\mathrm{j,cat}}^{\mathrm{eff}} \left.\frac{\partial P_j^{\mathrm{cat}}}{\partial r}\right|_{r=r_{\mathrm{p}}^{\mathrm{cat}}} = k_{\mathrm{gs},j}^{\mathrm{cat}} \left(P_{j,\mathrm{g}} - P_{j,\mathrm{s}}^{\mathrm{cat}}\right) \tag{26}$$

$$-\lambda_{\mathrm{cat}}^{\mathrm{eff}} \left.\frac{\partial T_{\mathrm{cat}}}{\partial r}\right|_{r=r_{\mathrm{p}}^{\mathrm{cat}}} = \alpha_{\mathrm{gs}}^{\mathrm{cat}} \left(T_{\mathrm{cat}}^{\mathrm{s}} - T\right) \tag{27}$$

$$t > 0, r = 0 \quad \frac{\partial P_j^{\mathrm{cat}}}{\partial r} = 0 \quad \frac{\partial T_{\mathrm{cat}}}{\partial r} = 0 \tag{28}$$

$$t = 0, r > 0 \quad P_j^{\mathrm{cat}}(r,0) = P_{j,\mathrm{g}}^{\mathrm{in}} \quad T_{\mathrm{cat}}(r,0) = T^{\mathrm{in}} \tag{29}$$

In Eqs. 21–24, the effectiveness diffusion coefficient in the catalyst particle was evaluated with the following equation

$$D_{j,\mathrm{cat}}^{\mathrm{eff}} = D_j \frac{\varepsilon_{\mathrm{p}}^{\mathrm{cat}}}{\tau} \tag{30}$$

The kinetics of glycerol steam reforming over bimetallic Co–Ni/Al_2O_3 catalyst was summarized with the following rate equation developed by Cheng et al.,[40] based on a Langmuir-Hinshelwood dual-site mechanism involving molecular adsorption of both reactants

$$r_{\mathrm{ref}} = \frac{k_{\mathrm{rxn}} P_{\mathrm{C_3H_8O_3}} P_{\mathrm{H_2O}}}{\left(1 + K_{\mathrm{C_3H_8O_3}} P_{\mathrm{C_3H_8O_3}}\right)\left(1 + K_{\mathrm{H_2O}} P_{\mathrm{H_2O}}\right)} \tag{31}$$

where

$$k_{\mathrm{rxn}} = 0.010471 \exp\left(-\frac{69,360}{RT}\right) \tag{32}$$

$$K_{\mathrm{C_3H_8O_3}} = 8.2125 \times 10^{-3} \exp\left(\frac{2931.4}{T}\right) \tag{33}$$

$$K_{\mathrm{H_2O}} = 0.379 \exp\left(-\frac{1904.4}{T}\right) \tag{34}$$

Porous Adsorbent Particle Scale Model—Mass and Heat Balance Equations. In the adsorbent particles, all components, without CO_2, are inert, and only one mass balance equation is solved in addition to the energy equation

$$\varepsilon_{\mathrm{p}}^{\mathrm{ads}} \frac{\partial P_{\mathrm{CO_2}}^{\mathrm{ads}}}{\partial t} = D_{\mathrm{CO_2,ads}}^{\mathrm{eff}} \frac{1}{r^2} \frac{\partial}{\partial r}\left(r^2 \frac{\partial P_{\mathrm{CO_2}}^{\mathrm{ads}}}{\partial r}\right) - \rho_{\mathrm{p}}^{\mathrm{ads}} r_{\mathrm{ads}} R T_{\mathrm{ads}} \tag{35}$$

$$\left(\varepsilon_{\mathrm{p}}^{\mathrm{ads}} \rho_{\mathrm{g}} c_{\mathrm{pg}} + \rho_{\mathrm{p}}^{\mathrm{ads}} c_{\mathrm{ps}}\right) \frac{\partial T_{\mathrm{ads}}}{\partial t} = \lambda_{\mathrm{ads}}^{\mathrm{eff}} \frac{1}{r^2} \frac{\partial}{\partial r}\left(r^2 \frac{\partial T_{\mathrm{ads}}}{\partial r}\right) + (-\Delta H_{\mathrm{R,ads}}) r_{\mathrm{ads},N} \rho_{\mathrm{p}}^{\mathrm{ads}} \tag{36}$$

The corresponding boundary and initial conditions are given as

$$t > 0, \quad r = r_{\mathrm{p}}^{\mathrm{ads}} \quad D_{j,\mathrm{ads}}^{\mathrm{eff}} \left.\frac{\partial P_{\mathrm{CO_2}}^{\mathrm{ads}}}{\partial r}\right|_{r=r_{\mathrm{p}}^{\mathrm{ads}}} = k_{\mathrm{gs,CO_2}}^{\mathrm{ads}} \left(P_{\mathrm{CO_2,g}} - P_{\mathrm{CO_2,s}}^{\mathrm{ads}}\right) \tag{37}$$

$$-\lambda_{\mathrm{ads}}^{\mathrm{eff}} \left.\frac{\partial T_{\mathrm{ads}}}{\partial r}\right|_{r=r_{\mathrm{p}}^{\mathrm{ads}}} = \alpha_{\mathrm{gs}}^{\mathrm{ads}} \left(T_{\mathrm{ads}}^{\mathrm{s}} - T\right) \tag{38}$$

Table 1. Mass- and Heat-Transfer Correlations

Parameter	Equation
Gas–solid mass-transfer coefficient—Chilton-Colburn analogy[41]	$k_{\mathrm{gs},j} = \frac{0.725 v_{\mathrm{sg}}}{Re_{\mathrm{g}}^{0.41-0.15}} Sc_j^{-2/3}$, where $Re_{\mathrm{g}} = \frac{v_{\mathrm{sg}} d_{\mathrm{p}} \rho_{\mathrm{g}}}{\mu_{\mathrm{g}}}$ and $Sc_j = \frac{\mu_{\mathrm{g}}}{\rho_{\mathrm{g}} D_{j,\mathrm{g}}}$
Gas–solid particle heat-transfer coefficient[42]	$\frac{\alpha_{\mathrm{gs}} d_{\mathrm{p}}}{\lambda_{\mathrm{g}}} = 2 + 0.6 Pr_{\mathrm{g}}^{1/3} \left(Re_{\mathrm{g}}/\varepsilon\right)^{1/2}$, where $Re_{\mathrm{g}} = \frac{v_{\mathrm{sg}} d_{\mathrm{p}} \rho_{\mathrm{g}}}{\mu_{\mathrm{g}}}$ and $Pr_{\mathrm{g}} = \frac{\mu_{\mathrm{g}} c_{\mathrm{pg}}}{\lambda_{\mathrm{g}}}$
Heat-transfer coefficient between gas phase and reactor wall—Leva correlation[43]	$\frac{h_{\mathrm{w}} d}{\lambda_{\mathrm{g}}} = 3.5 \left(\frac{d_{\mathrm{p}} v_{\mathrm{sg}} \rho_{\mathrm{g}}}{\mu_{\mathrm{g}}}\right)^{0.7} \exp\left(-4.6 \frac{d_{\mathrm{p}}}{d}\right)$

$$t > 0, r = 0 \quad \frac{\partial P_{\mathrm{CO_2}}^{\mathrm{ads}}}{\partial r} = 0 \quad \frac{\partial T_{\mathrm{ads}}}{\partial r} = 0 \tag{39}$$

$$t = 0, r > 0 \quad P_{\mathrm{CO_2}}^{\mathrm{ads}}(r,0) = P_{\mathrm{CO_2,g}}^{\mathrm{in}} \quad T_{\mathrm{ads}}(r,0) = T^{\mathrm{in}} \tag{40}$$

The molar rate of CO_2 removal per kilogram of CaO, , in the *N*th cycle can be represented as a function of fractional conversion of CaO

$$r_{\mathrm{ads},N} = \frac{1}{M_{\mathrm{CaO}}} \frac{dX_N}{dt} \tag{41}$$

Model Parameters' Estimation. The correlations for mass- and heat-transfer coefficients are listed in Table 1. The effective diffusion coefficients were evaluated assuming a tortuosity factor of 3. The molecular gas diffusivity coefficients in multicomponent gas mixtures were calculated with Blanc correlation[44]

$$D_j = \left(\sum_{\substack{i=1 \\ i \neq j}}^{n} \frac{y_i}{D_{ij}}\right)^{-1} \tag{42}$$

Diffusion coefficients for binary gas systems are predicted with Chapman and Enskog equation[44]

$$D_{ij} = 1.858 \times 10^{-3} T^{3/2} \frac{\left[\left(M_i + M_j\right)/M_i M_j\right]^{1/2}}{P \sigma_{ij}^2 \Omega_{ij}} \tag{43}$$

where

$$\sigma_{ij} = \frac{\sigma_i + \sigma_i}{2} \quad \sigma_j = \frac{2.3551 - 0.087\omega_j}{\left(P_{c,j}/T_{c,j}\right)^{1/3}} \tag{44}$$

$$\Omega_{ij} = \frac{A}{\left(T_{ij}^*\right)^B} + \frac{C}{\exp\left(DT_{ij}^*\right)} + \frac{E}{\exp\left(FT_{ij}^*\right)} + \frac{G}{\exp\left(HT_{ij}^*\right)} \quad T_{ij}^* = \frac{kT}{\varepsilon_{ij}} \tag{45}$$

$$\frac{\varepsilon_j}{kT_{\mathrm{c},j}} = 0.7915 + 0.1693\omega_j \quad \varepsilon_{ij} = \left(\varepsilon_i \varepsilon_j\right)^{1/2} \tag{46}$$

Knudsen diffusion coefficient was evaluated using the following correlation[45]

$$D_{kj} = \frac{2\bar{r}}{3} \left[\frac{8RT}{\pi M_j}\right]^{0.5}$$

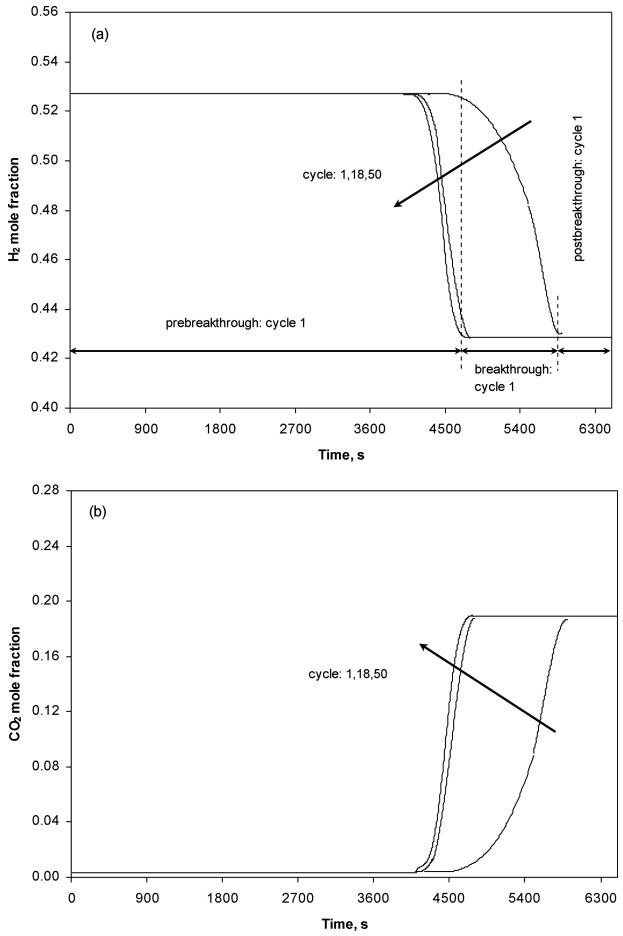

Figure 2. Outlet H_2 mole fraction (a) and CO_2 mole fraction (b) during cyclic sorption-enhanced steam glycerol reforming process.

Thermal conductivity of the gas mixture was estimated using Wassiljewa equation[44]

$$\lambda_g = \sum_{i=1}^{n} \frac{y_i \lambda_{i,g}}{\sum_{j=1}^{n} y_i \phi_{ij}}$$

$$\text{where } \phi_{ij} = \frac{\left[1 + \left(\mu_{i,g}/\mu_{j,g}\right)^{1/2} \left(M_j/M_i\right)^{1/4}\right]^2}{\left[8\left(1 + M_i/M_j\right)\right]^{1/2}} \tag{48}$$

Thermal conductivity of the species j in gas phase was estimated using Chung et al. correlation[44]

$$\lambda_{j,g} = 3.75 \frac{\varphi_j R \mu_{j,g}}{M_j} \tag{49}$$

where

$$\varphi_j = 1 + A_{p,j} \times \frac{0.215 + 0.28288A_{p,j} - 1.061B_{a,j} + 0.26665\left(2 + 10.5\left(\frac{T}{T_{c,j}}\right)^2\right)}{0.6366 + B_{a,j}\left(2 + 10.5\left(\frac{T}{T_{c,j}}\right)^2\right) + 1.061A_{p,j}B_{a,j}} \tag{50}$$

$$A_{p,j} = \frac{C_{p,j}}{R} - \frac{3}{2} \tag{51}$$

$$B_{a,j} = 0.7862 - 0.7109\omega_j + 1.3168\omega_j^2 \tag{52}$$

Viscosity of the gas mixture was estimated using Wilke's approximation[44]

$$\mu_g = \sum_{i=1}^{n} \frac{y_i \mu_{i,g}}{\sum_{j=1}^{n} y_i \phi_{ij}}$$

$$\text{where } \phi_{ij} = \frac{\left[1 + \left(\mu_{i,g}/\mu_{j,g}\right)^{1/2} \left(M_j/M_i\right)^{1/4}\right]^2}{\left[8\left(1 + M_i/M_j\right)\right]^{1/2}} \tag{53}$$

Viscosity of the species j in gas phase was estimated using the correlation of Chapman and Enskog[44]

$$\mu_{j,g} = 26.69 \times 10^{-7} \frac{\left(M_j T\right)^{0.5}}{\Omega_j \sigma_j^2} \tag{54}$$

where the diffusion collision integral and the characteristic length were evaluated with the Eqs. 44 and 45.

Effective thermal conductivity of the catalyst and adsorbent particles was evaluated with the porous solid model developed by Harriott[46]

$$\lambda_{cat(ads)}^{eff} = \lambda_s \frac{1 - \varepsilon_p}{\tau} \tag{55}$$

The effective axial bed conductivity in the axial direction was evaluated using the correlation of Yagi et al.[47]

$$\frac{\lambda_z^{eff}}{\lambda_g} = \beta \frac{1 - \varepsilon}{\frac{\lambda_g}{\lambda_s} + \varphi} + 0.75 Pr_g Re_p$$

$$\text{where } Re_p = \frac{v_{sg} d_p \rho_g}{\mu_g} \quad \text{and} \quad Pr_g = \frac{\mu_g c_{pg}}{\lambda_g} \tag{56}$$

The extent of back-mixing in the gas phase was quantified in terms of an axial dispersion coefficient that was evaluated using the correlation of Edwards and Richardson[48]

Table 2. Base Case Fixed-Bed Reactor Operating Conditions

Operating Conditions	Data
Reactor diameter	0.025 m
Fixed-bed height	1.0 m
Catalyst particle density	1200 kg/m^3
Catalyst particle porosity	0.45
Adsorbent particle density	1670 kg/m^3
Adsorbent particle porosity	0.5
Voidage of the fixed bed	0.39
Catalyst particle diameter	0.002 m
Adsorbent particle diameter	0.002 m
Adsorbent/catalyst volume ratio	4
Inlet reactor temperature	873 K
Reactor pressure	0.1 MPa
Inlet superficial gas velocity	0.1 m/s
Feed conditions	
Glycerol partial pressure	10 kPa
H_2O partial pressure	91.3 kPa

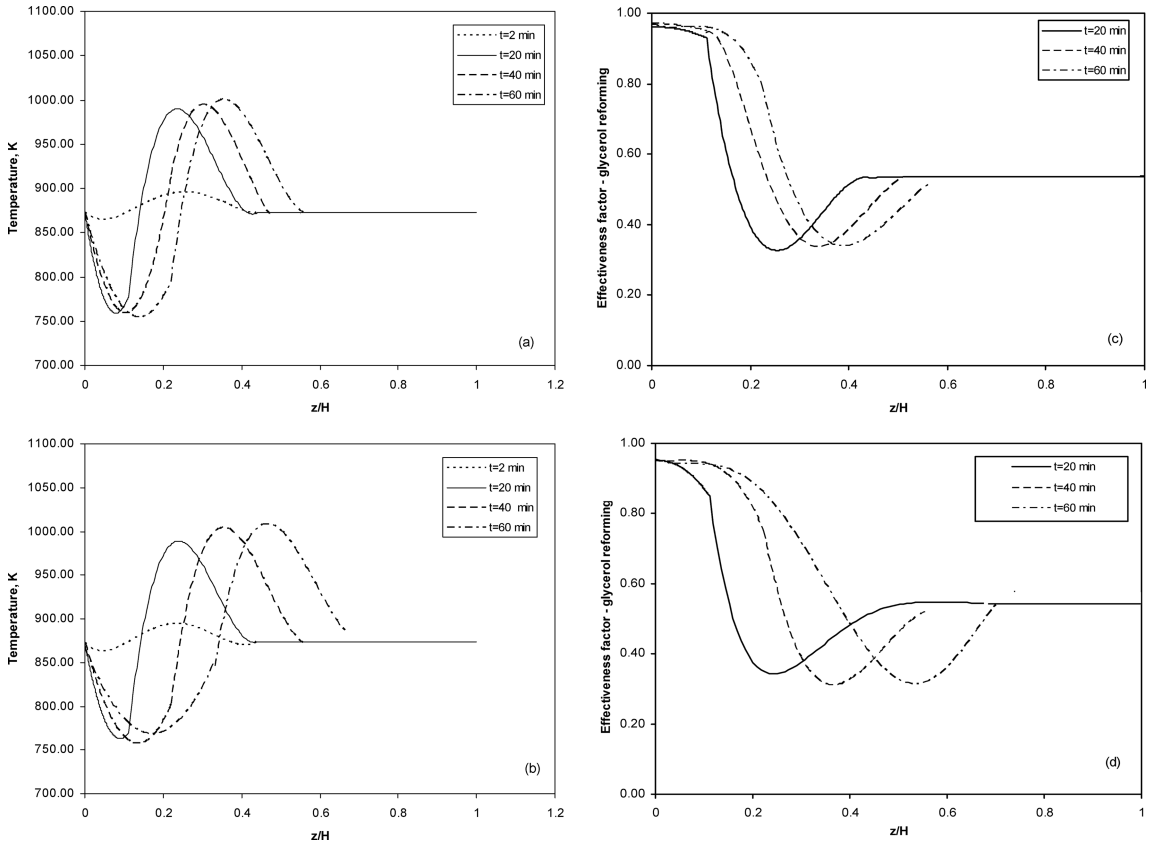

Figure 3. Time-dependent spatial distribution of fixed-bed reactor temperature and glycerol reforming effectiveness factor during cyclic sorption-enhanced steam glycerol reforming process: (a) and (c) cycle 1 and (b) and (d) cycle 18.

$$D_g = 0.73D_j + \frac{0.5u_g\varepsilon_g d_p}{1 + 9.49D_j/(u_g\varepsilon_g/d_p)} \tag{57}$$

Method of Solution. To solve the system of partial differential equations, we discretized in space and solved the resulting set of ordinary differential equations. The spatial discretization is performed using the standard cell-centered finite difference scheme (at the reactor level) and the method of orthogonal collocation[49] (at the solid particles level). The number of collocation points specified for the catalyst particles was restricted to 8. The GEAR integration method for stiff differential equations was used to integrate the time derivatives. The relative error tolerance for the time integration process in the present simulations is set at 10^{-7} for each time step. Fortran 77 software on Intel® Core™ 2 Duo Processor E7500 was used to generate the numerical platform.

Results and Discussion

The sorption-enhanced steam glycerol reforming reactor model was initially used to predict the performance of cyclic (in practical applications CO_2 adsorption and desorption are repeated in numerous cycles) sorption-enhanced reforming process in a fixed-bed reactor (Figure 2). The fixed-bed reactor operating conditions are given in Table 2. In Figure 2a, the reaction time of sorption-enhanced steam glycerol reforming process is divided into three regions. The pre-breakthrough is a high-purity hydrogen period characterized by a match between CO_2 formation rate and CO_2 adsorption rate—for cycle 1 the hydrogen mole fraction (dry basis) is

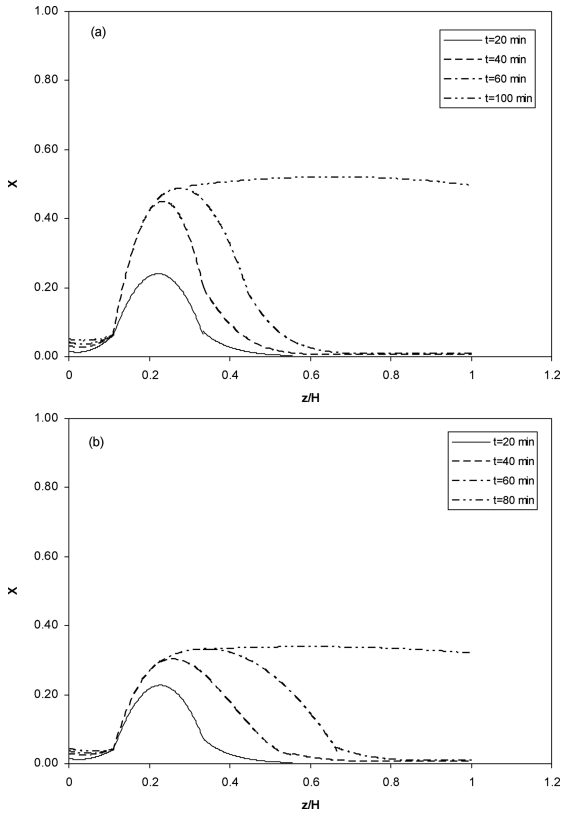

Figure 4. Time-dependent axial distribution of adsorbent conversion: (a) cycle 1 and (b) cycle 18.

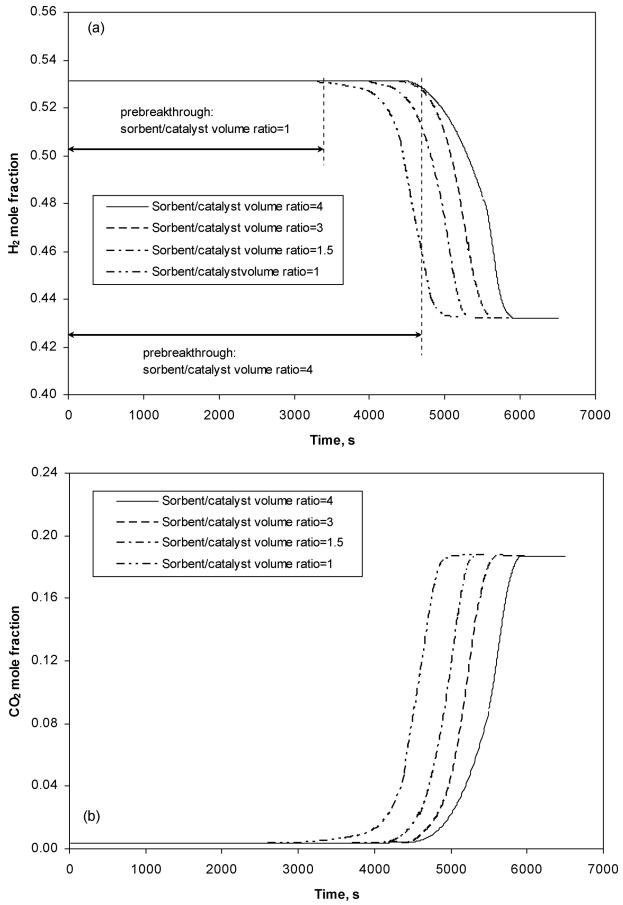

Figure 5. Outlet H_2 mole fraction (a) and CO_2 mole fraction (b) during sorption-enhanced steam glycerol reforming process at different values of adsorbent/catalyst volume ratio (cycle number 1).

higher than 99% during 80 min (the simulation results follow the experimental data of He et al.[50]). In this period, steam glycerol reforming and CO_2 removal occur at maximum efficiency and the concentration of each component in the product gas is very near to the respective equilibrium values.[23] In the breakthrough period, the CO_2 removal efficiency of the adsorbent begins to decrease resulting in a decrease/increase in the H_2/CO_2 content (Figures 2a and 2b). When the adsorbent approaches its maximum conversion, CO_2 removal is no longer effective, and the postbreakthrough period begins. Only steam glycerol reforming reactions occur in this period. The simulated results show that the operation time of producing high-purity hydrogen declines with the increase of the cyclic number due to the adsorbent activity loss. However, the duration of the sorption-enhanced period can last a long time at a large cyclic number due to the high reactivity and stability of Ca-based adsorbent. From the 50th cycle number, the prebreakthrough time will remain constant, because the adsorbent reaches the final residual capture capacity.[23] The ultimate prebreakthrough time is very important in designing and operating of sorption-enhanced steam glycerol reforming process and is dependent on the nature of adsorbent and its thermal stability on cyclic operation. Ca-based adsorbent developed in this work has a slow decline of sorption capacity, resulting in a high final prebreakthrough time.

The thermal behavior of sorption-enhanced reforming process and glycerol reforming effectiveness factor are shown in Figure 3 (a wall temperature of 873 K was used to heat the reactor). In the entrance region of the reactor, the temperature rapidly drops, because the endothermic steam glycerol reforming reaction in this region is faster than the exothermic CO_2 adsorption reaction, resulting in a large temperature decrease. The temperature decline in the entrance region of the reactor lasts a long period of time. In the

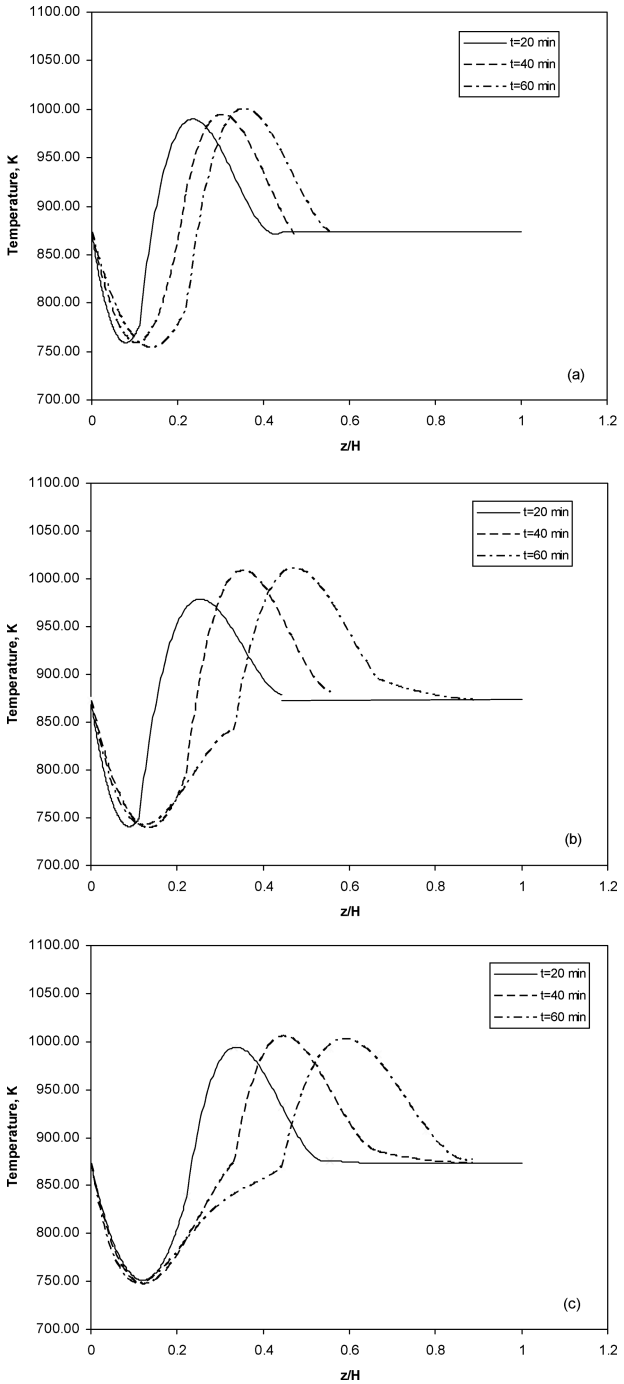

Figure 6. Reactor temperature as function of time and space for different values of adsorbent/catalyst volume ratio (cycle number 1): (a) adsorbent/catalyst volume ratio = 4; (b) adsorbent/catalyst volume ratio = 1.5; and (c) adsorbent/catalyst volume ratio = 1.

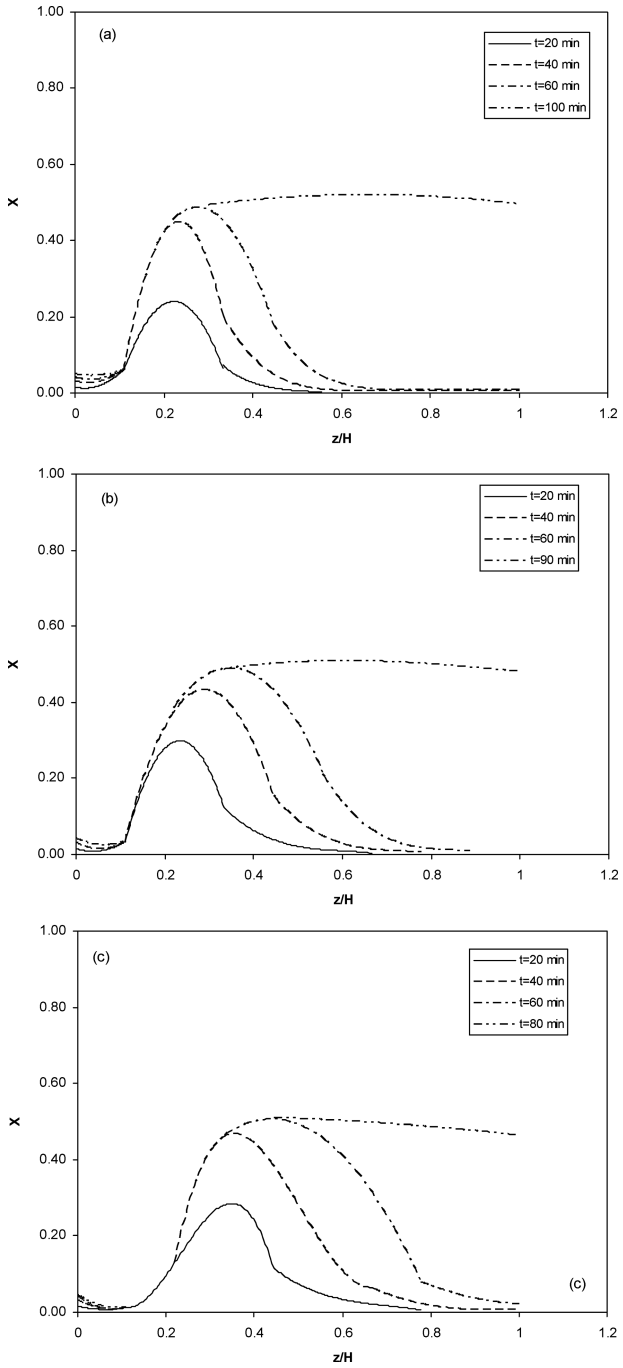

Figure 7. Time-dependent axial distribution of adsorbent conversion (cycle number 1): (a) adsorbent/catalyst volume ratio = 4; (b) adsorbent/catalyst volume ratio = 1.5; and (c) adsorbent/catalyst volume ratio = 1.

succeeding fixed-bed reactor location after this cool bed region, the CO_2 adsorption reaction is dominant: the heat generated in CO_2 adsorption reaction is used to heat up this region, and, therefore, the local temperature of the fixed-bed region increases. A maximum increase in temperature to 130 K above the initial temperature can be observed, and the fixed-bed zone with such a temperature raise moves toward the reactor exit with the increase of reaction time. With the increase of cyclic number, the fixed-bed reactor zones with a low temperature extend and the bed zones with a maximum in temperature move quickly, which explains the decrease of the operation time of producing high-purity hydrogen.

Figure 4 shows typical, unsteady-state axial profiles of adsorbent conversion for cyclic sorption-enhanced reforming process (two cyclic numbers were used in simulation). In the entrance region of the reactor, adsorbent conversion is not significant because of the low temperature that gives low CO_2 adsorption rate. After the cool fixed-bed reactor region, fractional adsorbent conversion increases due to the heat generated in CO_2 adsorption process and the bed zone with maximum in conversion moves toward the reactor exit with the increase of reaction time following the temperature profile. It should be noted that the adsorbent approaches its maximum conversion after 100 min for cycle number 1 and, respectively, 80 min for cycle number 18. At this reaction time CO_2 removal is no longer effective and the postbreakthrough period begins. At higher cyclic number, the mass of $CaCO_3$ formed during the sorption-enhanced reforming process is lower due to the loss of the sorbent activity.

Sorption-enhanced steam glycerol reforming is an integrated process involving steam glycerol reforming reaction and *in situ* CO_2 adsorption. When CO_2 formation rate relates with CO_2 adsorption rate, the advantage of adsorbent on reaction becomes obvious. The relationship between the two processes depends on the adsorbent/catalyst ratio. Thus, simulations were undertaken to study the effect of the

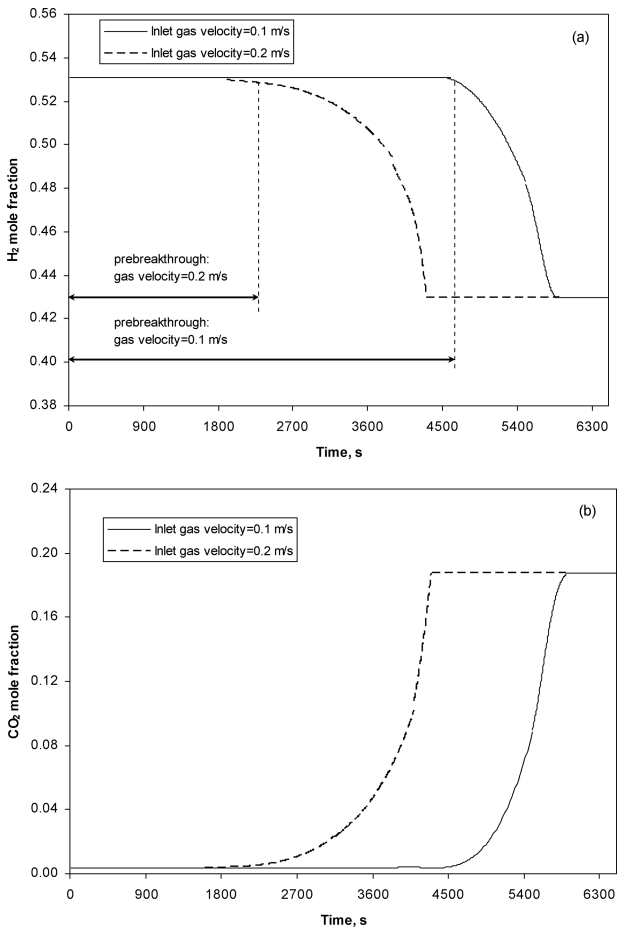

Figure 8. Outlet H_2 mole fraction (a) and CO_2 mole fraction (b) during sorption-enhanced steam glycerol reforming process at different values of inlet gas velocity (cycle number 1).

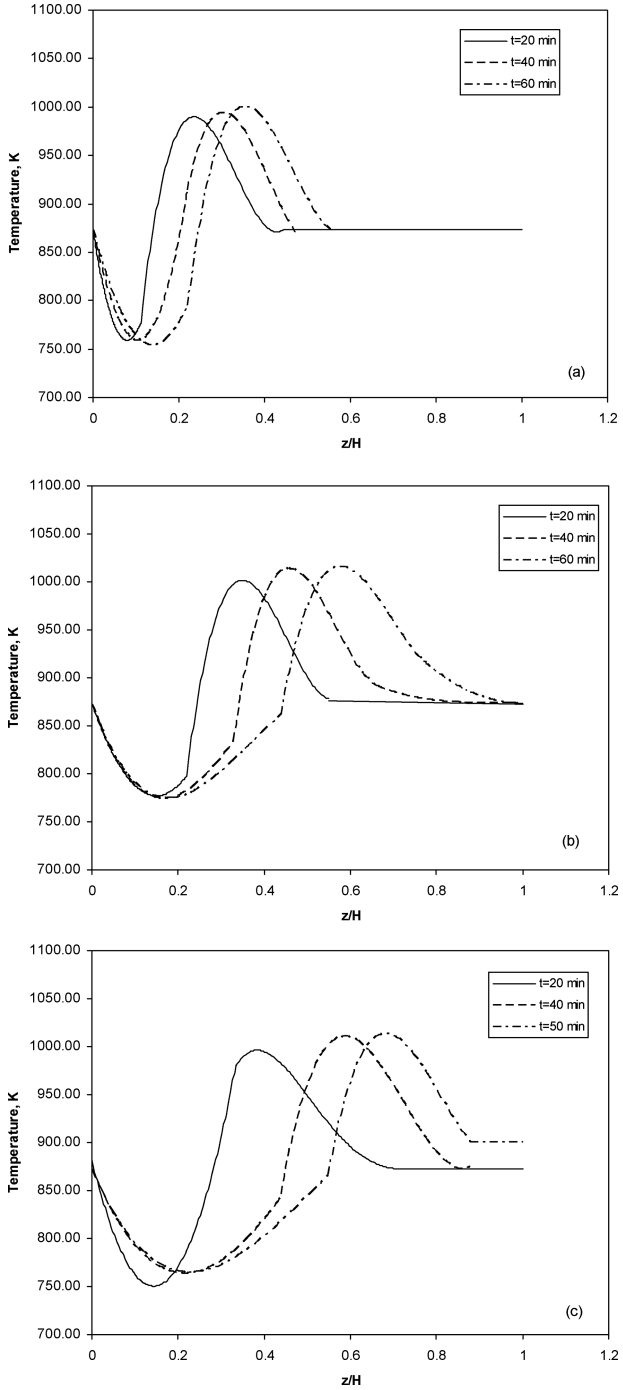

Figure 9. Reactor temperature as function of time and space for different values of inlet superficial gas velocity (cycle number 1): (a) v_{sg} = 0.1 m/s; (b) v_{sg} = 0.15 m/s v_{sg} = 0.15 m/s; and (c) v_{sg} = 0.2 m/s.

adsorbent/catalyst volume ratio on the sorption-enhanced steam glycerol reforming process. The adsorbent/catalyst volume ratio was selected to provide the operating conditions, which assure that steam glycerol reforming reaction is not the limiting step (CO_2 production rate from steam glycerol reforming is higher than the CO_2 adsorption rate). Figure 5 shows that the operational time of the reactor before the breakthrough declines with the decrease of the volume fraction of adsorbent in fixed-bed reactor due to the decrease of the adsorption capacity of the adsorbent (dry basis H_2 mole fraction is higher than 99% during 80 min for a adsorbent/catalyst volume ratio of 4 and 54 min for a adsorbent/catalyst volume ratio of 1). Also, because CO_2 sorption capacity is strongly influenced by temperature (overall kinetics is favored at higher temperature), the thermal behavior of sorption-enhanced steam glycerol reforming process (Figure 6) plays a significant role in the magnitude of the hydrogen high-purity time period: CO_2 sorption capacity decreases with the decrease of the adsorbent/catalyst volume ratio and due to the relatively insufficient amount of adsorbent at the reactor inlet, the low-temperature bed zone enlarges, and the bed zones with a maximum in temperature move quickly toward the reactor exit with the increase of reaction time. Following the thermal regime, the entrance region of the reactor with low adsorbent conversion expands with the diminution of adsorbent/catalyst volume ratio (Figure 7). Also, at lower adsorbent/catalyst volume ratio, the reactor zones with a maximum in adsorbent conversion move quickly toward the reactor exit with the increase of reaction time, and adsorbent approaches its maximum conversion after a smaller period of time (80 min for a adsorbent/catalyst volume ratio of 1 and, respectively, 100 min for a adsorbent/catalyst volume ratio of 4).

Higher inlet superficial gas velocity gives shorter prebreakthrough period (Figure 8). At high-gas throughputs, CO_2 production rate in the glycerol reforming process is

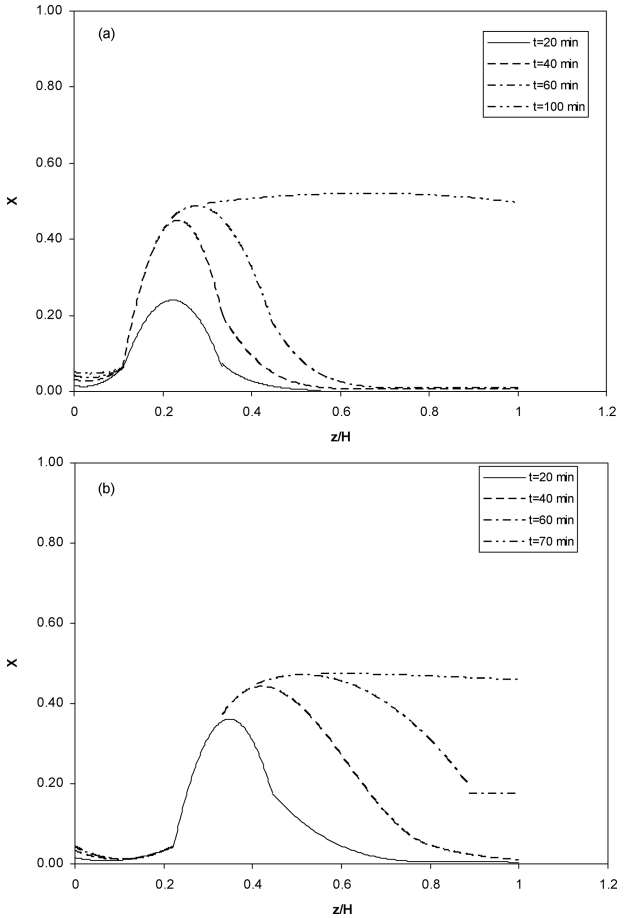

Figure 10. Time-dependent axial distribution of adsorbent conversion for different values of inlet superficial gas velocity (cycle number 1): (a) v_{sg} = 0.1 m/s and (b) v_{sg} = 0.2 m/s.

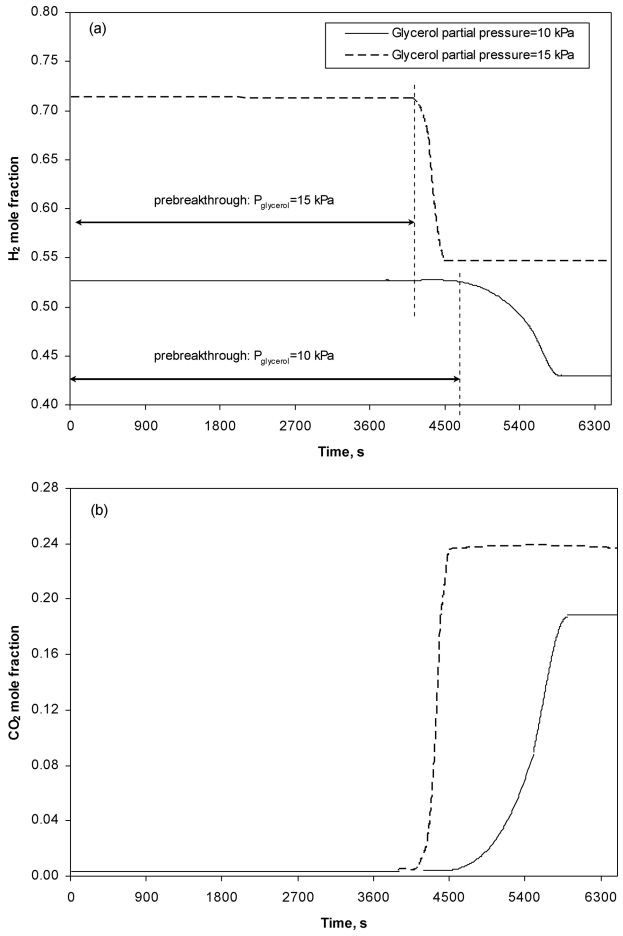

Figure 11. Outlet H_2 mole fraction (a) and CO_2 mole fraction (b) during sorption-enhanced steam glycerol reforming process at different values of glycerol partial pressure (cycle number 1).

higher than CO_2 adsorption rate of the adsorbent. As result, CO_2 removal efficiency of the adsorbent begins to decrease after a small period of time due to the high amount of CO_2 generated in steam glycerol reforming process, and the high concentration of H_2 cannot be sustained for a long time. The prebreakthrough period with dry basis H_2 mole fraction higher than 99% diminishes from 80 min (inlet superficial gas velocity = 0.1 m/s) to 60 min (inlet superficial gas velocity = 0.15 m/s) and then to 40 min (inlet superficial gas velocity = 0.2 m/s). By comparing the time and space temperature and adsorbent conversion profiles when inlet superficial gas velocity is increased (Figures 9 and 10), respectively, adsorbent/catalyst volume ratio is decreased (Figures 6 and 7), it can be concluded that the thermal behavior of sorption-enhanced steam glycerol reforming process is qualitatively similar, because in both circumstances the integrated system is limited by the adsorption capacity of the adsorbent: at high inlet superficial gas velocity CO_2 removal efficiency begins to decrease after a small period of time due to the relatively insufficient amount of adsorbent to sustain the high CO_2 production rate in glycerol reforming process and as result, the low-temperature bed zone enlarges and the bed zones with a maximum in temperature move quickly toward the reactor exit with the increase of reaction time. At higher inlet superficial gas velocity, adsorbent approaches its maximum conversion after a smaller period of time (70 min for $v_{sg} = 0.2$m/s and 100 min for $v_{sg} = 0.1$m/s).

Simulations were undertaken to study the influence of the glycerol partial pressure on the sorption-enhanced steam glycerol reforming process. The glycerol partial pressure was selected to provide the operating conditions that assure that steam glycerol reforming reaction is not the limiting step and carbon deposition, methane production, and pyrolysis are not significant (steam-to-glycerol ratio higher than 4).[40] Higher glycerol partial pressure (lower steam-to-glycerol ratio) gives shorter prebreakthrough period (Figure 11): the prebreakthrough period with dry H_2 mole fraction higher than 99% diminishes at 70 min when glycerol partial pressure is increased to 15 kPa (the simulation results follow the experimental data of He et al.[50]). With the increase of glycerol partial pressure, the integrated system is limited by the adsorption capacity of the adsorbent: CO_2 removal efficiency of the adsorbent decreases due to the high amount of CO_2 generated in steam glycerol reforming process and the operational time of the reactor before the breakthrough declines. Consequently, the time and space temperature and adsorbent conversion profiles (Figure 12) have similar trends as in the case, when inlet superficial gas velocity is increased or adsorbent/catalyst volume ratio is decreased.

Figure 13 shows the influence of the inlet reactor temperature on the sorption-enhanced steam glycerol reforming process. At high inlet reactor temperature (923 K in our case), CO_2 adsorption process is limited by the higher value of the

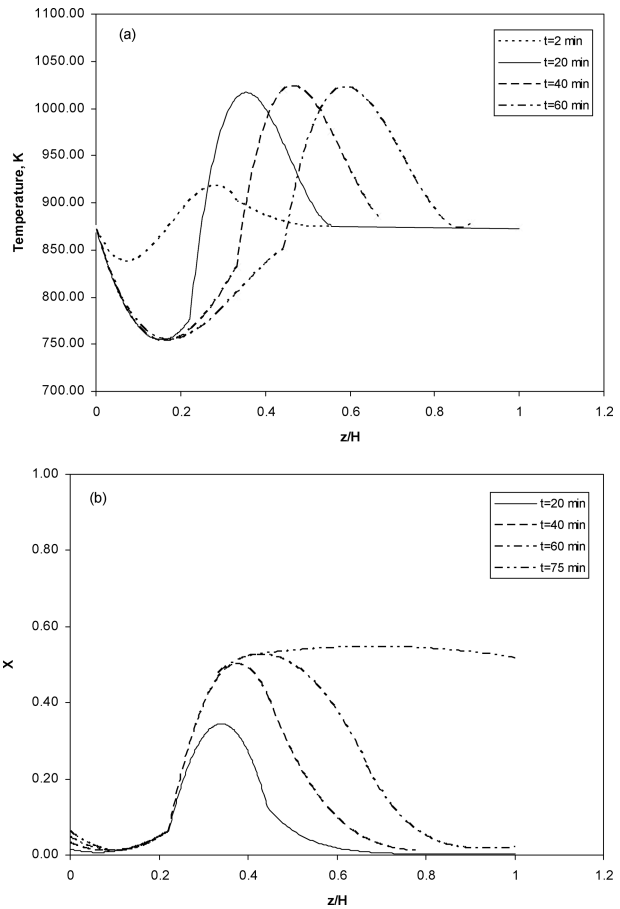

Figure 12. Reactor temperature (a) and adsorbent conversion (b) as function of time and space for $P_{C_3H_8O_3}$ = 15 kPa (cycle number 1).

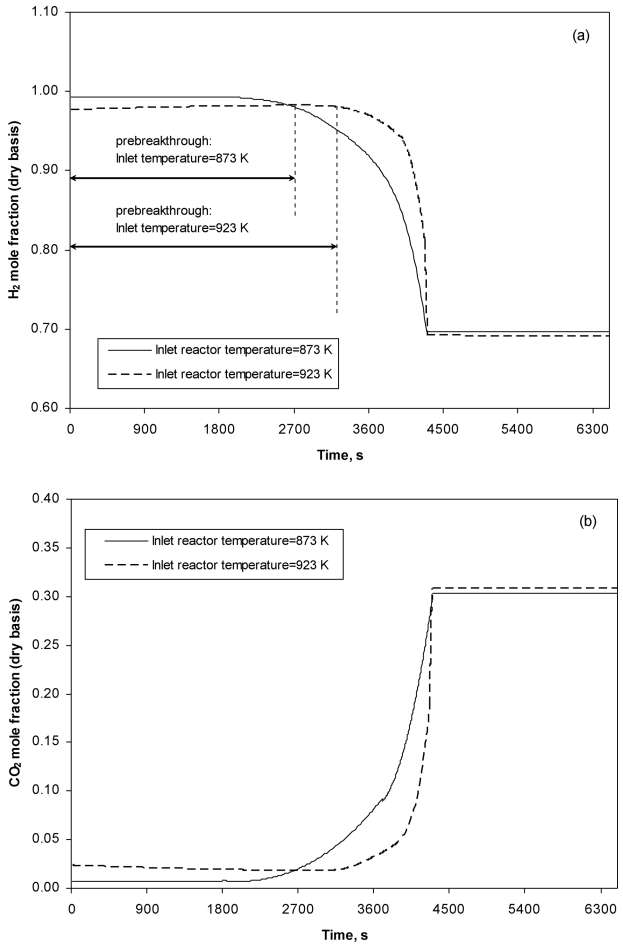

Figure 13. Outlet dry basis H_2 mole fraction (a) and CO_2 mole fraction (b) during sorption-enhanced steam glycerol reforming process at different values of inlet reactor temperature (cycle number 1).

equilibrium CO_2 partial pressure, and the dry basis H_2 mole fraction cannot be higher than 99%. Consequently, in Figure 13, the prebreakthrough period was considered the operational time with a dry basis H_2 mole fraction higher than 98%. The prebreakthrough period increases with the increase of the inlet temperature; however, the purity of H_2 is lower. The thermal behavior of sorption-enhanced steam glycerol reforming process controls the size of the hydrogen high-purity time period: CO_2 sorption capacity increases with the increase of the inlet temperature, because fixed-bed reactor zones with a low-temperature contract, the bed zones with a maximum in temperature move slowly toward the reactor exit with the increase of reaction time and in the second part of the reactor the temperature is higher (Figure 14). The increase of adsorption capacity is confirmed mainly by the contraction of the entrance region of the reactor with low adsorbent conversion (not shown).

Conclusions

Sorption-enhanced steam glycerol reforming provides a promising alternative for single-stage production of hydrogen with a high purity. In this work, we investigated this integrated process in a fixed-bed reactor highlighting the effect of the key operating parameters on the process performance. A two-scale, nonisothermal, unsteady-state model has been developed to account for gas dynamics whereupon were tied steam glycerol reforming/CO_2 capture kinetics, thermodynamics, thermal effects, and variable gas flow rate due to chemical and physical contractions. A new Ca-based adsorbent material recently developed from natural limestone was used in this work, and the kinetics of CO_2 capture has been investigated experimentally and described by a mathematical reaction-rate model.

Gas throughputs and adsorbent/catalyst ratio have a major influence on the operational time of producing high-purity hydrogen characterized by a match between CO_2 formation rate and CO_2 adsorption rate. At high gas velocity, CO_2 production rate in glycerol reforming process is higher that CO_2 adsorption rate of the adsorbent and as result, CO_2 removal efficiency begins to decrease after a small period of time and the high concentration of H_2 cannot be sustained for a long time. The operational time of producing high-purity hydrogen can be enhanced by increasing the adsorbent/catalyst volume ratio, by adding steam to the reaction system and by increasing the inlet reactor temperature. The high-purity hydrogen period declines with the increase of the cyclic number due to the adsorbent activity loss. However, the Ca-based adsorbent used in this work has a slow decline of sorption capacity, resulting in a high ultimate prebreakthrough time, which is very important in designing and operating of sorption-enhanced steam glycerol reforming process.

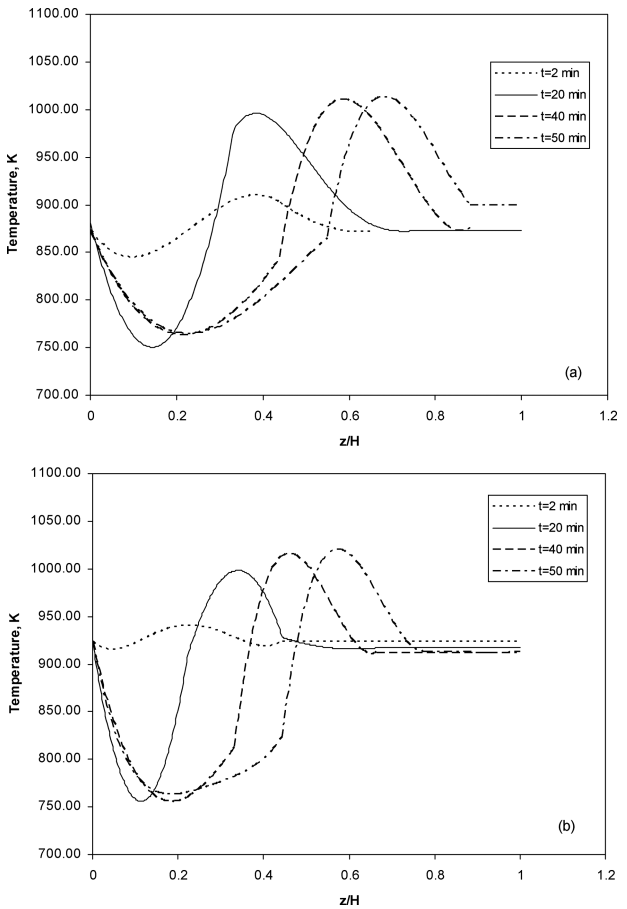

Figure 14. Reactor temperature as function of time and space for different values of inlet reactor temperature (cycle number 1): (a) T^{in} = 873 K and (b) T^{in} = 923 K.

Sorption-enhanced steam glycerol reforming process minimizes the amount of waste by-products and represents an energy efficient alternative for producing hydrogen—the overall energy balance is favorable, because exothermic CO_2 adsorption provides the heat to endothermic steam glycerol reforming, and extra energy is required only in the process of adsorbent regeneration. Furthermore, it presents an opportunity to improve the economics of green hydrogen production by reducing the cost as the processing steps required for subsequently CO_2 separation are removed.

Acknowledgments

Financial supports from Natural Sciences and Engineering Research Council of Canada (NSERC), FRQNT Centre in Green Chemistry and Catalysis (CGCC), and Centre de Recherche sur les Propriétés des Interfaces et sur la Catalyse (CERPIC), Laval University, are gratefully acknowledged.

Notation

a_s = bed specific surface area, m^2/m^3_{solid}
c_{pg} = specific heat capacity of gas phase, J/(kg K)
c_{ps} = specific heat capacity of solid phase, J/(kg K)
$C_{p,j}$ = heat capacity of species j, J/(mol K)
d = reactor diameter, m
d_p = particle diameter, m
D_g = axial dispersion coefficient in the gas phase, m^2/s
D_{ij} = molecular diffusivity coefficient for binary gas systems, m^2/s
D_j = molecular gas diffusivity coefficient in multicomponent gas mixture, m^2/s
D_j^{eff} = effective diffusivity of species j inside the particle, m^2/s
E_1, E_2 = Ergun constants
f_{ads} = volume fraction of adsorbent in fixed bed
f_{cat} = volume fraction of catalyst in fixed bed
h_w = heat-transfer coefficient in the vicinity of the wall, J/(m^2 s K)
k = Boltzmann constant
k_{gs} = gas–solid mass-transfer coefficient, m/s
k_{rxn} = reaction rate constant, kmol/($kg_{cat}kPa^2$ s)
$K_{C_3H_xO_3}$ = glycerol adsorption constant, kPa^{-1}
K_{H_2O} = steam adsorption constant, kPa^{-1}
K_T = overall bed-wall heat-transfer coefficient, J/(m^2 s K)
M_j = molecular mass of species j, kg/kmol
M_g = molecular mass of the gas mixture, kg/kmol
P = reactor pressure, Pa
P_c = critical pressure, Pa
P_j = partial pressure of species j, Pa
$r_{ads,N}$ = CO_2 removal rate, kmol/(kg_{ads} s)
r_i = reaction rate, kmol/($kg_{cat(ads)}$ s)
r_{ref} = glycerol reforming reaction rate, kmol/(kg_{cat} s)
R = ideal-gas constant
t = time, s
T = temperature, K
T_c = critical temperature, K
T_r = reduced temperature (t/t_c)
T_w = reactor wall temperature, K
u_g = average interstitial velocity of gas phase, m/s
v_{sg} = superficial velocity of gas phase, m/s
X = fractional conversion of adsorbent
X_N = fractional conversion of adsorbent in the Nth cycle
y_j = mole fraction of species j in gas phase
z = axial coordinate, m

Greek letters

α_{gs} = gas–particle heat-transfer coefficient, J/(m^2 s K)
ε_g = gas-phase holdup
ε_p = particle porosity
η_i = effectiveness factor for reaction i
λ_g = thermal conductivity of gas phase, J/(m s K)
λ_g = thermal conductivity of species j in gas phase, J/(m s K)
$\lambda_{j,g}$ = axial effective thermal conductivity, J/(m s K)
λ_x^{eff} = effective thermal conductivity of adsorbent particles, J/(m s K)
λ_{ads}^{eff} = effective thermal conductivity of catalyst particles, J/(m s K)
λ_{cat}^{eff} = thermal conductivity of the solid phase, J/(m s K)
μ_g = dynamic viscosity of gas phase, kg/(m s)
$\mu_{j,g}$ = dynamic viscosity of species j in gas phase
ρ_g = density of gas phase, kg/m^3
ρ_p = particle density,
ρ_{sc} = catalyst and adsorbent bed density, kg/m^3
σ_{ij} = characteristic length, Å
τ = tortuosity factor
μ_j = stoichiometric coefficient
ω = acentric factor
Ω_{ij} = diffusion collision integral

Subscripts

ads = adsorbent particle
cat = catalyst particle
g = gas phase
i = inert gas
in = reactor inlet
ref = reforming
s = solid phase, surface of the catalyst (adsorbent) particle

Literature Cited

1. Cortright RD, Davda RP, Dumesic JA. Hydrogen from catalytic reforming of biomass-derived hydrocarbons in liquid water. *Nature*. 2002;418:964–967.
2. Hu X, Lu G. Investigation of the steam reforming of a series of model compounds derived from bio-oil for hydrogen production. *Appl Catal B*. 2009;88:376–385.
3. Saxena RC, Adhikari DK, Goyal HB. Biomass-based energy fuel through biochemical routes: a review. *Renewable Sustainable Energy Rev*. 2009;13:167–178.
4. Fermoso J, He L, Chen D. Sorption enhanced steam reforming (SESR): a direct route towards efficient hydrogen production from biomass-derived compounds. J Chem Technol Biotechnol. 2012;87:1367–1374. DOI 10.1002/jctb.3857.
5. Wu G, Zhang C, Li S, Huang Z, Yan S, Wang S, Ma X, Gong J. Sorption enhanced steam reforming of ethanol on Ni–CaO–Al_2O_3 multifunctional catalysts derived from hydrotalcite-like compounds. Energy Environ Sci. 2012;5:8942–8949. DOI: 10.1039/c2ee21995f.
6. Hirai T, Ikenanga N-O, Miyake T, Suzuki T. Production of hydrogen by steam reforming of glycerin on Ruthenium catalyst. Energy Fuels. 2005;19:1761–1762.
7. Dou B, Dupont V, Rickett G, Blakeman N, Williams PT, Chen H, Ding Y, Ghadiri M. Hydrogen production by sorption-enhanced steam reforming of glycerol. *Bioresour Technol*. 2009;100:3540–3547.
8. Douette AMD, Turn SQ, Wang W, Keffer VI. Experimental investigation of hydrogen production from glycerin reforming. *Energy Fuels*. 2007;21:3499–3504.
9. Mackaluso JD. The use of syngas derived from biomass and waste products to produce ethanol and hydrogen, MMG 445 Basic Biotechnol eJ. 2007;3:98–103.
10. Dauenhauer PJ, Salge JR, Schmidt LD. Renewable hydrogen by autothermal steam reforming of volatile carbohydrates. *J Catal*. 2006;244:238–247.
11. Dou B, Dupont V, Williams PT, Chen H, Ding Y. Thermogravimetric kinetics of crude glycerol. *Bioresour Technol*. 2008;100:2613–2620.
12. Valliyappan T, Bakhshi NN, Dalai AK. Pyrolysis of glycerol for the production of hydrogen or syn gas. *Bioresour Technol*. 2008;99:4476–4483.
13. Hashaikeh R, Butler IS, Kozinski JA. Selective promotion of catalytic reactions during biomass gasification to hydrogen. *Energy Fuel*. 2006;20:2743–2746.
14. Vaidya PD, Rodrigues AE. Glycerol reforming for hydrogen production: a review. *Chem Eng Technol*. 2009;32:1463–1469.
15. Lee KB, Beaver MG, Caram HS, Sircar S. Production of fuel-cell grade hydrogen by thermal swing sorption enhanced reaction concept. *Int J Hydrogen Energy*. 2008;33:781–790.
16. Harrison DP. Sorption-enhanced hydrogen production: a review. *Ind Eng Chem Res*. 2008;47:6486–6501.
17. Mayorga JR, Sircar S. Sorption-enhanced reaction process for hydrogen production. *AIChE J*. 1999;45:248–256.
18. Ding Y, Alpay E. Adsorption-enhanced steam methane reforming. *Chem Eng Sci*. 2000;55:3929–3940.
19. Kinoshita CM, Turn SQ. Production of hydrogen from bio-oil using CaO as a CO_2 sorbent. *Int J Hydrogen Energy*. 2003;28:1065–1071.

20. Yi KB, Harrison DP. Low-pressure sorption-enhanced hydrogen production. Ind Eng Chem Res. 2005;44:1665–1669.
21. Ochoa-Fernandez E, Rusten HK, Jakobsen HA, Ronning M, Holmen A, Chen D. Sorption enhanced hydrogen production by steam methane reforming using Li_2ZrO_3 as sorbent: sorption kinetics and reactor simulation. *Catal Today*. 2005;106:41–46.
22. Lee KB, Beaver MG, Caram HS, Sircar S. Novel thermal-swing sorption-enhanced reaction process concept for hydrogen production by low temperature steam-methane reforming. *Ind Eng Chem Res*. 2007;46:5003–5014.
23. Li, ZS, Cai NS. Modeling of multiple cycles for sorption-enhanced steam methane reforming and sorbent regeneration in fixed bed reactor. *Energy Fuels*. 2007;21:2909–2918.
24. Lee DK, Baek, IH, Yoon, WL. Modeling and simulation for the methane steam reforming enhanced by in situ CO_2 removal utilizing the CaO carbonation for H_2 production. *Chem Eng Sci*. 2004;59:931–942.
25. Essaki K, Muramatsu T, Kato M. Effect of equilibrium shift by using lithium silicate pellets in methane steam reforming. *Int J Hydrogen Energy*. 2008;33:4555–4559.
26. Reijers HTJ, Boon J, Elzinga GD, Cobden PD, Haije WG, van den Brink RW. Modeling study of the sorption-enhanced reaction process for CO_2 capture. *I. Model development and validation*. *Ind Eng Chem Res*. 2009;48:6966–6974.
27. Kapil A, Bhat SA, Sadhukhan J. Multiscale characterization framework for sorption enhanced reaction processes. *AIChE J*. 2008;54:1025–1036.
28. Barelli L, Bidini G, Gallorini F, Servili, S. Hydrogen production through sorption-enhanced steam methane reforming and membrane technology: a review. *Energy*. 2008;33:554–570.
29. Halabi MH, de Croon MHJM, van der Schaaf J, Cobden PD, Schouten JC. Kinetic and structural requirements for a CO_2 adsorbent in sorption enhanced catalytic reforming of methane—Part I: Reaction kinetics and sorbent capacity. *Fuel*. 2012;99:154–164.
30. Chen HS, Zhang T, Dou B, Dupont V, Williams PT, Ghadiri M, Ding Y. Thermodynamic analyses of adsorption enhanced steam reforming of glycerol for hydrogen production. *Int J Hydrogen Energy*. 2009;34:7208–7222.
31. Li Y, Wang W, Chen B, Cao Y. Thermodynamic analysis of hydrogen production via glycerol steam reforming with CO_2 adsorption. *Int J Hydrogen Energy*. 2010;35:7768–7777.
32. Albrecht KO, Wagenbach KS, Satrio JA, Shanks BH, Wheelock TD. Development of a CaO-based CO_2 sorbent with improved cyclic stability. *Ind Eng Chem Res*. 2008;47:7841–7848.
33. Radfarnia HR, Iliuta MC. Development of zirconium-stabilized calcium oxide absorbent for cyclic high-temperature CO_2 capture. *Ind Eng Chem Res*. 2012;51:10390–10398.
34. Li L, King DL, Nie Z, Howard Ch. Magnesia-stabilized calcium oxide absorbents with improved durability for high temperature CO_2 capture. *Ind Eng Chem Res*. 2009;48:10604–10613.
35. Rusten HK, Ochoa-Fernandez E, Lindborg H, Chen D, Jakobsen HA. Hydrogen production by sorption-enhanced steam methane reforming using lithium oxides as CO_2-acceptor. *Ind Eng Chem Res*. 2007;46:8729–8737.
36. Lee DK. An apparent kinetic model for the carbonation of calcium oxide by carbon dioxide. *Chem Eng J*. 2004;10:71–82.
37. Johnsen K, Grace J, Elnashaie S, Kolbeinsen L, Eriksen D. Modeling of sorption-enhanced steam reforming in a dual fluidized bubbling bed reactor. *Ind Eng Chem Res*. 2006;45:4133–4143.
38. Grasa GS, Abanades JC. CO_2 capture capacity of CaO in long series of carbonation/calcination cycles. Ind Eng Chem Res. 2006;45:8846–8851.
39. Baker EH. The calcium oxide-carbon dioxide system in the pressure range 1–300 atm. *J Chem Soc*. 1962;70:464–470.
40. Cheng CK, Foo SY, Adesina AA. Glycerol steam reforming over bimetallic Co–Ni/Al_2O_3. *Ind Eng Chem Res*. 2010;49:10804–10817.
41. Aris R. *Introduction to the Analysis of Chemical Reactors*. New Jersey: Prentice-Hall, 1965.
42. Ranz E. Friction and transfer coefficients for single particles and packed beds. *Chem Eng Progr*. 1952;48:247–253.
43. Froment GF, Bischoff KB. Chemical Reactor Analysis and Design, 2nd ed. New York: Wiley, 1990.
44. Reid RC, Prausnitz JM, Poling BE. The Properties of Gases and Liquids, 4th ed. New York: McGraw Hill, 1987.
45. Treybal RE. Mass Transfer Operations, 2nd ed. New York: McGraw Hill, 1968.
46. Harriott P. Thermal conductivity of catalyst pellets and other porous particles. *Part I: Review of models and published results. Chem Eng J*. 1975;10:65–71.
47. Yagi S, Kunii D, Wakao N. Studies on axial effective thermal conductivities in packed beds. *AIChE J*. 1960;6:543–546.
48. Edwards MF, Richardson JF. Gas dispersion in packed beds. *Chem Eng Sci*. 1968;23:109–123.
49. Finlayson BA. *The Method of Weighted Residuals and Variational Principles*. New York: Academic Press, 1972.
50. He L, Parra MS, Blekkan EA, Chen D. Towards efficient hydrogen production from glycerol by sorption enhanced steam reforming. *Energy Environ Sci*. 2010;3:1046–1056.

Manuscript received May 28, 2012, and revision received Sept. 18, 2012.